Antenna Design and Simulation

David Alvarez Outerelo, Francisco Javier Diaz Otero, Nelson Pinto
EI Telecomunicacion, Campus Universitario s/n 36310 Vigo Spain

THIS chapter describes the design and simulation of several prototype antennas at different operation frequencies, analyzing their advantages and disadvantages. The main objective of this chapter is to provide possible antenna designs that allow the generated symbols to be transmitted by radio frequency in bands corresponding to the emerging 6G systems [Rap19]. Two possible implementations are described: on-chip antennas and external antennas to the PIC in microstrip technology. The work presented is theoretical for chip-integrated antennas since there was not enough budget to deal with its manufacture and there is also no experimental characterization system. However, off-chip antenna designs have been able to be manufactured and measured in a special anechoic chamber for small-sized, high-frequency antennas.

In **section 4.1**, general questions are discussed as a preliminary step to the design, such as the selected frequency bands and the chosen technologies. In **section 4.2,** a two on-chip antenna models are introduced. **Section 4.3** is dedicated to the off-chip antenna models.

4.1 General considerations

The objective initially proposed in this Thesis was to provide the CV-QKD transmitter with a radiofrequency transmission channel in addition to the optical output channel. Although the initial design frequency of the transmitter is 10GHz, the phase modulators can reach a higher modulation rate up to 35 GHz. The availability of two parallel transmission channels opens up the field of application of the proposed transmitter.

Since the designed CV-QKD transmitter is fully resettable it could be configured to transmit ten photons per symbol by simply increasing the laser power and diverting the power to the main waveguide via the variable splitters.

Two types of solutions are possible to radiate the output signal:

- *on-chip antenna*: the developed antenna could be integrated into the transmitter PIC itself or into an individual chip, on an InP or Si platform. Millimeter band values must be chosen as working frequencies. These high values of frequency allow to have effective wavelengths in the substrate small enough to be able to integrate the antenna design in an individual chip and even in the PIC of the transmitter. The achieved designs will have a limited power gain and can only be used in short-range applications.
- *off-chip antenna*: if longer ranges are required, the design must seek a technology that allows higher power gains to be achieved. Therefore, larger antennas will be achieved that must be located externally to the PIC. Microstrip technology appears to be the most suitable to achieve the requirements of millimeter band applications, such as the 60GHz band, in a compact size.

Except for the case of an antenna integrated in the transmitter PIC, and therefore operating in a lower frequency band than that given by the photodiodes, it is necessary to have intermediate circuitry between the PIC output and the designed antenna if bands of frequency higher than 35GHz. This intermediate circuitry would include elements to allow the output signal from the RF output of the transmitter to be upconverted to the higher frequency band of interest. Among other elements, this circuitry should require a mixer, filters, amplifiers and impedance matching balun.

The upconverter could be integrated with the antenna itself or be an additional chip. Wire bonding is required to connect these new chips (antenna w or without upconverter) to the InP transmitter PIC. An example of the connection via wire bonding is illustrated by **Figure 4.1**.

For future testing of antennas designed that will not be integrated within the transmitter PIC due to the higher frequency band to operate in, it was developed a printed circuit or PCB that enables the PIC to be connected by wire bonding to a series of coplanar microstrip lines matched in impedance to 50 Ohms which in turn will be connected to the antenna or upconverter chip.

The high complexity of the transmitter due to the number of outputs and inputs to be controlled simultaneously also makes it necessary to carry out the PIC packaging, since in the measurement setup it is impossible to have all the necessary RF and DC probes at the same time due to the reduced dimensions of the transmitter micropositioners.

Therefore, the PCB shown in **Figure 4.2** has been designed, which will be manufactured and connected to the chip using wire bonding both for a future complete characterization of the transmitter and for testing in antennas whose frequency is higher than the modulation baseband.

A 3D model of the final packaging was also made with the radio frequency and fiber optic outputs necessary for the correct operation of the transmitter, as shown in **Figure 4.3**.

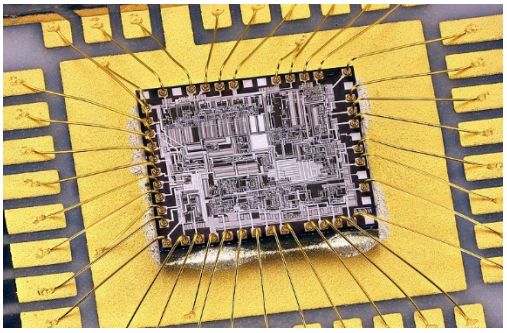

Figure 4.1. Example of wire bonding between a PIC and a support PCB.

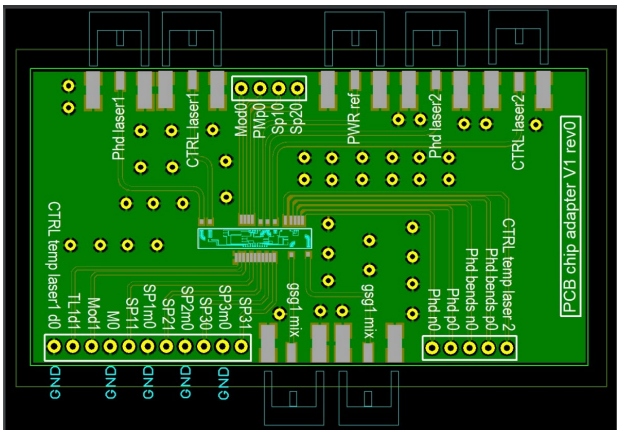

Figure 4.2. Support PCB with transmitter layout.

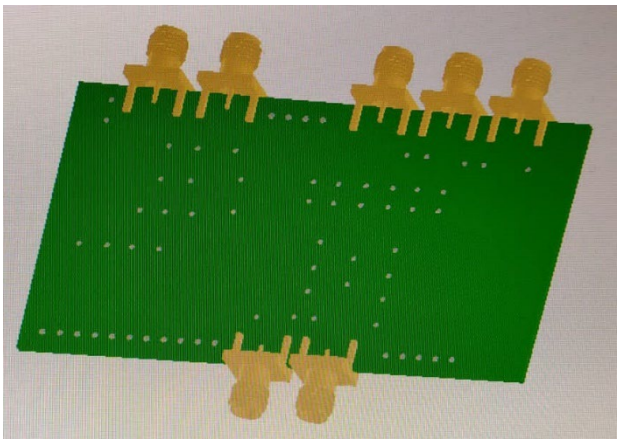

Figure 4.3. Support PCB with transmitter layout.

4.2 On-chip integrated antenna design

In this section, the two on-chip antenna designs are presented. The first design would allow its integration within the transmitter PIC and, therefore, would not require any type of connection or intermediate upconverter device. The frequency band of operation for this InP antenna was 26GHz allocated for satellite segment in 6G systems [Saa20] [Let19] [Gio20].

The second design is proposed to be integrated in quartz, including a Graphene radiating patch. The operation frequency for this model was set to 1 THz.Federal Communications Commission decided to release frequencies from 95 GHz to 3 THz for potential use in mobile communications, with up to 21 GHz for unlicensed use [IEE][FCC]. At THz wave bands, numerous design challenges arise to achieve a reasonable trade-off between technological design issues and commercial criteria - low cost, small size, radiation efficiency, antenna gain, broadband performance, real-time reconfigurable features, and so on [Yu13] [Han08] [Gom12] [Hwa08] [Car12] [Car13].

The two models of on-chip integrated antennas were composed by a rectangular microstrip patch and a microstrip feed line, disposed on InP or quartz substrate with relative dielectric constant ϵ_r of 9.61 and 3.75, respectively. This simple structure is generally used as basic radiation element for building an array antenna. This unit cell shows an input impedance of 140Ω, to make it compatible with the power dividers used in the feeding network connecting the single radiating elements of an array antenna.

In Figure 4.4 it is depicted the geometry of the antenna, with the rectangular patch and the feedline designed at an objective center frequency. The dimensions L_W and P_l determine the center frequency [Luo13] [Poz08] [Alv15] of the radiating patch. For a regular rectangular patch the edge input impedance is 144Ω. The dimensions F_W and F_l determine the center frequency of the feedline.

In absence of plasmonic modes, as in the upper THz range, there is no option for miniaturization, then and only the first fundamental mode of resonance of the rectangular patch can be used.

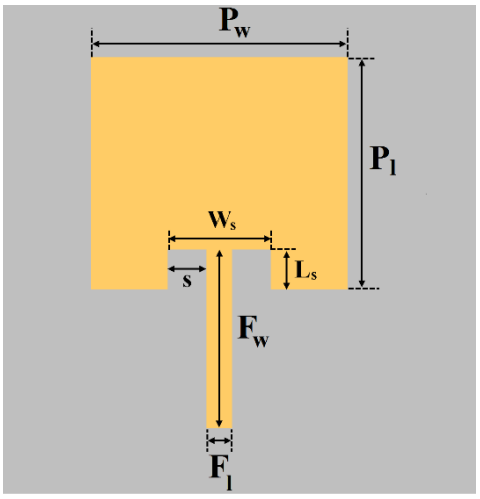

Figure 4.4. Geometry of the antenna with the rectangular radiating patch and the feedline.

The width of the patch P_w is given by (4.1):

$$P_W = \frac{c}{2f_r\sqrt{\frac{\epsilon_r+1}{2}}} \tag{4.1}$$

with f_r the desired resonance frequency and c the light speed in vacuum. The bandwidth of the antenna depends on the patch width P_W [Luo13] [Poz08] [Alv15], and thus on the value of ϵ_r. The simulation software will determine the relative dielectric constant ϵ_r of the material selected for the patch.

The effective dielectric constant ϵ_{eff} is given by (4.2):

$$\epsilon_{eff} = \frac{\epsilon_r+1}{2} + \frac{\epsilon_r-1}{2}\left(1 + \frac{12*h}{P_w}\right) \tag{4.2}$$

The length of the patch P_l is calculated from (4.3):

$$P_l = L_{eff} - (2 * \Delta L) \tag{4.3}$$

with ΔL is the fields overflow, and L_{eff} the effective length that is calculated as per (4.4):

$$L_{eff} = \frac{c}{2*f_r\sqrt{\epsilon_{eff}}} \tag{4.4}$$

The width of the feed line F_W is calculated from (4.5) in order to obtain a characteristic impedance of around 50 Ω:

$$F_W = h\left(\frac{377}{50\sqrt{\epsilon_r}} - 2\right) \tag{4.5}$$

First of all, a single Gold patch was designed on InP, and its performance was then contrasted with a hybrid graphene-gold patch on quartz. Following both antenna models are described in detail.

4.2.1 InP antenna

The design of an integrated antenna within the transmitter's own substrate, that is, InP, with a maximum thickness of 250 μm, has been carried out. The substrate is considered as a monolayer of InP with a refractive index value of 3.1 at 1 THz.

One of the main problems when designing antennas in this type of substrate is the low transmission frequency, for a transmission frequency, such as the one considered to be 26 GHz. For said resonance frequency, the effective wavelength in the substrate is of 3.45 millimeters, which is a great handicap when designing integrated antennas within the PIC itself, since the

measurements of the typical DIE chip in HHI only have the following standard dimensions: 2x8 mm (4000€), 4x8 mm (8000€) and 12x8 mm (24,000€).

These limited dimensions and high prices make it necessary to design simple antenna prototypes for short-range communication applications with the transmitter, in such a way that the design of antenna arrays, which would occupy a large part of the useful surface of the chip, is not necessary.

Therefore, the design of a rectangular patch antenna is proposed, which will be directly connected to the photodiode (1) of the Power Reference output. This type of connection will allow the data transmission by the CV-QKD transmitter, but not the reception of information from an external device, this is due to the fact that the photodiode only provides output current based on the optical power received, and not the other way around.

The design, simulation and subsequent optimization have been carried out using the CST MICROWAVE STUDIO electromagnetic simulation software, which allows simulations to be carried out in the time and frequency domain, discretizing the 3D structure in a series of base cells and propagating the electromagnetic field along of these.

Table 4.1. Dimensions of the InP on-chip integrated antenna.

Dimensions	Values
Relative dielectric permittivity, ϵ_r	9.61
Substrate width	6 mm
Substrate length	6 mm
Substrate thickness, ϵ_r	0.25 mm
Gold patch thickness	0.0035 mm
Feed line width, F_w	0.0246 mm
Feed line length, F_l	$0.35 \cdot \lambda$
Guide port dimensional factor	4.62
Wavelength, λ	3.45 mm
Patch length, P_l	$(\lambda/2) \cdot F_1$ mm
Patch width, P_w	$1.3 \cdot P_l$ mm
Inset feed width, W_s	$(F_w + 0.2) \cdot F_2$
Inset feed length, L_S	0.4 mm
F_1	1
F_2	1

The parameters for the patch geometry are summarized in Table 4.1. To perform the optimization, the length of the patch P_l and the width of the inset feed W_s are taken as variable parameters, being multiplied by two scale factors, F_1 and F_2, respectively, with the following objective:

- The factor F_1 by multiplying the length of the patch P_l causes the resonant frequency to

move towards the target value of 26 GHz, and

- the factor F_2 together with the variation of the length of the inset L_s feed allows an optimum adaptation of impedances to be achieved, measured in terms of the scattering parameter $s_{11}(f)$.

The output of the optimization process is shown in **Figure 4.5**. An s_{11} value of -32 dB was obtained at a frequency of 26GHz, with which it is considered that the optimization has achieved its objective, as shown in **Figure 4.6**.The optimal values achieved for F_1, F_2 and are summarized in **Table 4.2**.

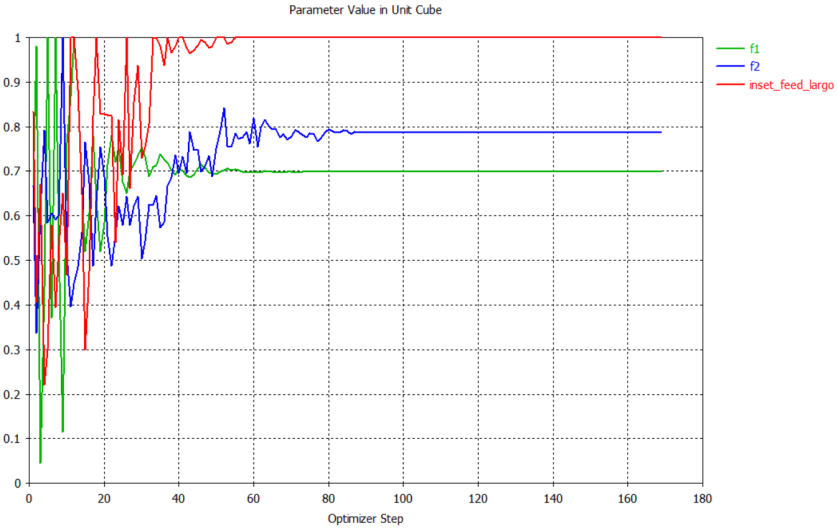

Figure 4.5. Optimization output for the InP PIC integrated antenna.

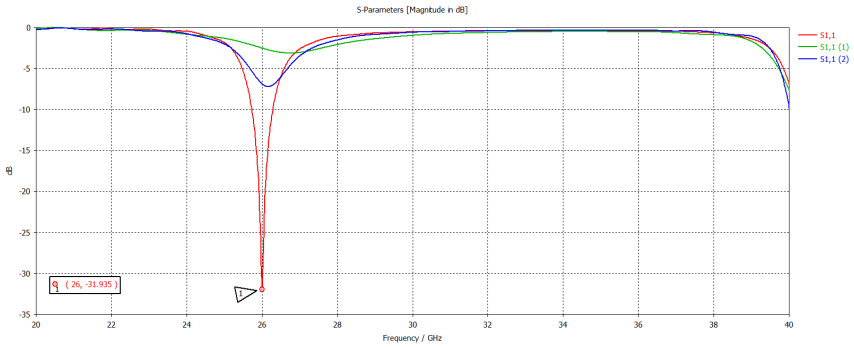

Figure 4.6. Evolution of s_{11}(@26GHz) during the design optimization: initial (green), intermediate (blue), and final (red).

Table 4.2. Optimal values of the optimization variable parameters.

Optimization variable parameter	Value
F_1	1.0095794039874
F_2	1.0361474785913
Inset feed length, L_s	0.6 mm

Finally, the simulation process is launched for the optimized values of inset feed length L_s and the patch length P_l. The main antenna features obtained are:

- a final value of s_{11} of -32 dB

- a bandwidth of 1.6 GHz
- a radiation pattern, for $\varphi = 0°$ cut plane, with a main lobe of 5 dB gain and a beamwidth of 100°.

The 3D radiation pattern for $\varphi = 0°$ cut plane is shown in **Figure 4.7**. Even though it is a simple design, it presents acceptable performance values for short-range transmission of information bits. In addition, it is a feasible and achievable design through a gold deposition process for the DC and RF clads in a PIC.

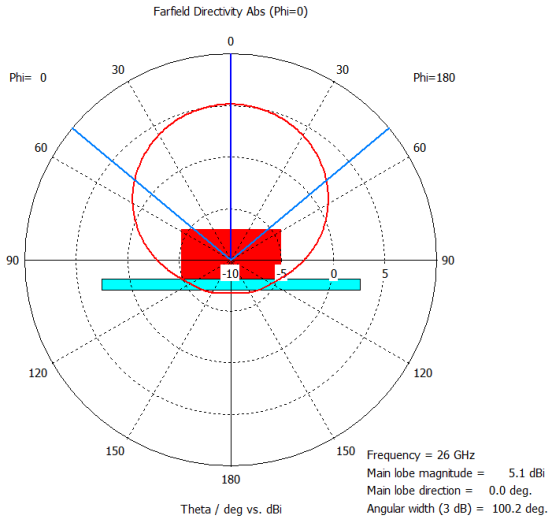

Figure 4.7. Optimization output for the InP PIC integrated antenna.

4.2.2 Hybrid Graphene antenna

This section describes the design and simulation of a Silicon platform antenna while exploring the properties of using a superconducting material such as Graphene.The antenna design bear in mind the use of the 6G band, in this case 1 THz as central frequency.

The base structure of the antenna is the same as the one described previous section but in this case with a graphene radiating cell consisted of a rectangular microstrip Graphene patch and a microstrip Gold feed line disposed on a quartz substrate with relative dielectric constant ϵ_r of 3.75. The 3D model onf the hybrid Graphene-Gold antenna is shown in in **Figure 4.8**.

For matching the impedances of the patch element of 140Ω and the feedline of 50Ω, the feedline does not join on the patch edge but in an interior point by using a rectangular notch. The feed line constitutes a cascade quarter wavelength impedance adapter, and its length F_l is calculated. The notch dimensions – *S*, *Ls* and *Ws* – condition the fine tuning of the impedance matching.

For simulating the graphene on CST Microwave Studio a new material was created as a tabulated surface impedance R_s, calculated a priori as in (4.1)-(4.4):

$$R_s(\omega, \mu_c, \gamma, T) = \frac{1}{\sigma(\omega, \mu_c, \gamma, T)} \qquad (\Omega) \tag{4.1}$$

$$\sigma(\omega, \mu_c, \gamma, T) = \sigma_{intra}(\omega, \mu_c, \gamma, T) + \sigma_{inter}(\omega, \mu_c, \gamma) \tag{4.2}$$

$$\sigma_{intra}(\omega, \mu_c, \gamma, T) = \frac{j e_c^2 K_B T}{\pi \hbar^2 (\omega - j2\gamma)} \left(\frac{\mu_c}{K_B T} + 2\ln\left(e^{\left(-\frac{\mu_c}{K_B T}\right)} + 1\right) \right) \tag{4.3}$$

$$\sigma_{inter}(\omega, \mu_c, \gamma) = \frac{-j e_c^2}{4\pi\hbar} ln\left(\frac{2|\mu_c| - (\omega - j2\gamma)\hbar}{2|\mu_c| + (\omega - j2\gamma)\hbar}\right) \tag{4.4}$$

One of the problems when implementing expressions (4.1)-(4.5) and verifying them is that some authors [Han08][Car13] consider the scattering rate given in electron-volts, or well the relaxation constant (τ_s) is provided instead of the scattering rate. Then, units can be swaped by using the following expressions (4.5)-(4.6):

$$\gamma(s^{-1}) = \frac{1}{2\tau_s} \tag{4.5}$$

$$\gamma(ev) = \frac{\hbar}{2\tau_s} \tag{4.6}$$

For a practical antenna design, actual values for γ and μ_c obtained from measurements should be required. The scattering rate γ value depends of the fabrication method of graphene – graphite exfoliation, vapor deposition or atomic layer deposition – and it would need to be measured to achieve a greater precision design. However some many authors take a value close to $0.11ev$ ($\tau_s = 5.98\ ps$) [Han08]. This value of the scattering rate γ is chosen to be approximately the same as for electron-acoustic phonon interactions in single-layer of carbon nanotubes [Ada07]. A typical value of the chemical potential is $\mu_c = 0.3ev$.

Assuming $T = 300\ K$, $\mu_c = 0.3ev, \tau_s = 1\ ps$ The graphene surface impedance R_s was calculated shown in **Figure 4.9**. It can be observed that it is practically imaginary: whilst the real part (resistance) shows a constant value over frequency, the imaginary component (reactance) is largely dependent on frequency. At 1THz and for $\mu_c = 0.3ev$, the value of R_s is $17 + j53.43$.

After a software optimization process to maximize the power gain, the optimal dimensions of the antenna were obtained. The dimensions of this antenna (in mm) are summarized in **Table 4.3**.

In **Figure 4.10** it can be observed that the optimized antenna presents a good impedance matching with a return loss $s_{11}(f)$ of -40 dB at the central frequency, and a bandwidth of 38 GHz taking a criterion of $|s_{11}(f)| \leq -10\text{dB}$. Typical values of bandwidth for a rectangular patch are found between two and four percent of the central frequency.

The 3D radiation pattern is presented in **Figure 4.11**, and the $\varphi = 0°$ cut plane in **Figure 4.12**, It presents a maximum gain of 6.14 dBi, beamwidth of 73°, and the main lobe direction at $\varphi = 0°$.

Table 4.3. Dimensions of the Graphene integrated antenna.

Dimensions	Values
Relative dielectric permittivity, ϵ_r	12
Substrate width	211.5 µm
Substrate length	179.54 µm
Substrate thickness, ϵ_r	10 µm
raphene patch thickness	0.0035 mm
Feed line width, F_w	18.93 µm
Feed line length, F_l	80 µm
Guide port dimensional factor	4.68
Wavelength, λ	3.45 mm
Patch length, P_l	90 µm

Patch width, P_w	117 µm
Inset feed width, W_s	38.93 µm
Inset feed length, L_S	24.6 µm
Input impedance	140 Ω

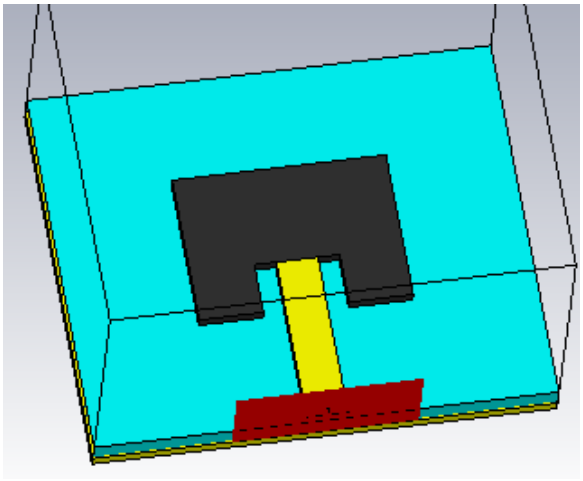

Figure 4.8. 3D antenna model with a graphene patch and a gold feedline.

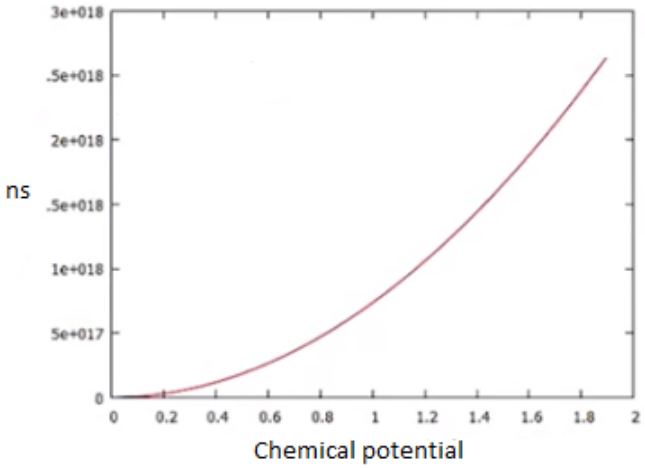

Figure 4.9. Surface charge density n_s vs chemical potential μ_c.

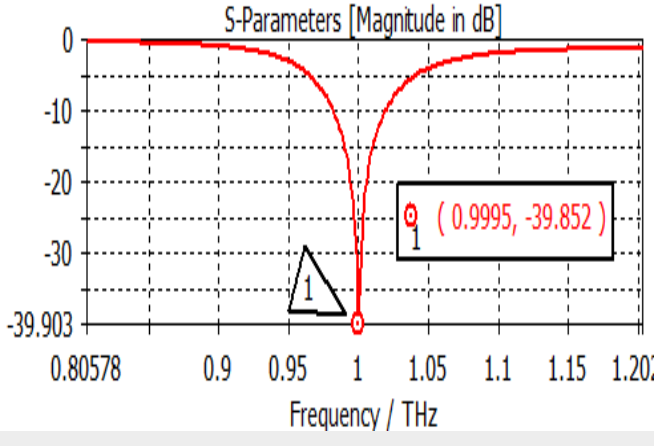

Figure 4.10. S_{11} of the hybrid graphene-gold antennas.

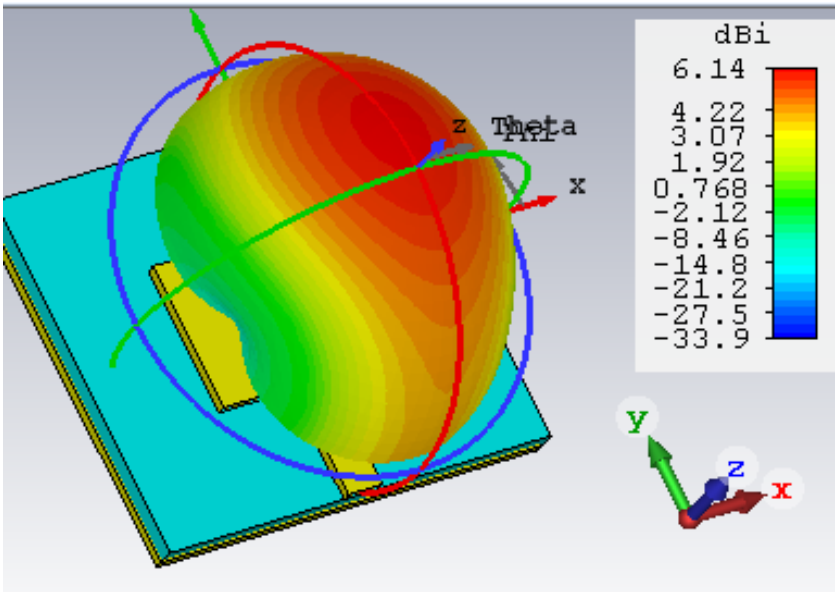

Figure 4.11. 3D radiation diagram of the hybrid graphene-gold antennas.

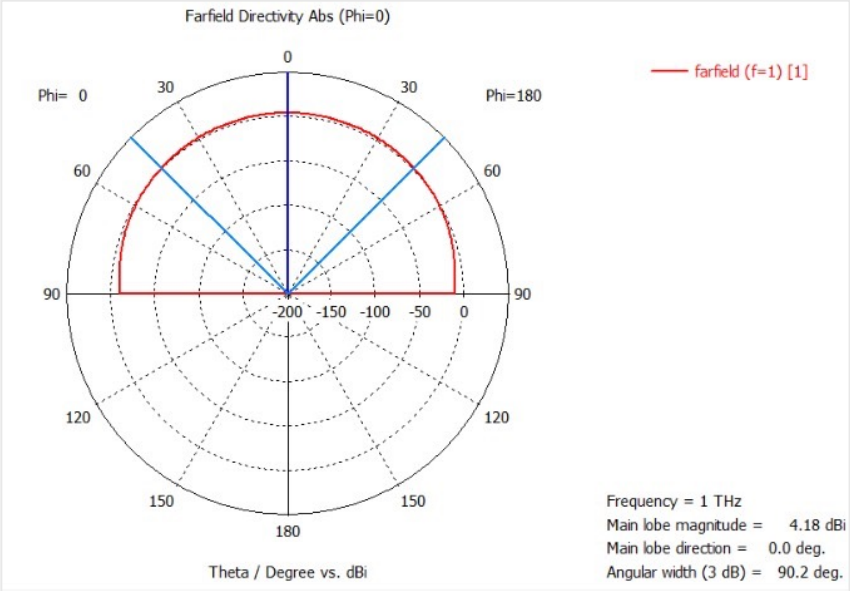

Figure 4.12. Radiation diagram of the hybrid graphene-gold antenna, cut plane of $\varphi = 0°$

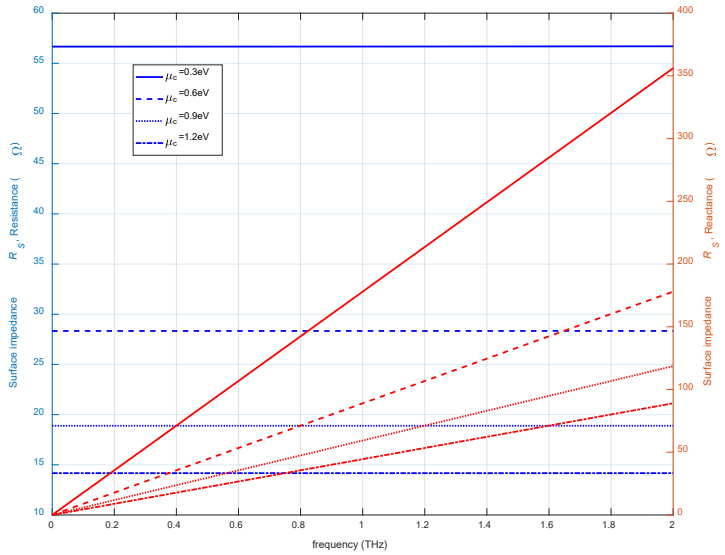

Figure 4.13. Resistence (blue) and reactance (red) of graphene surface impedance R_s for different values of chemical potential μ_c.

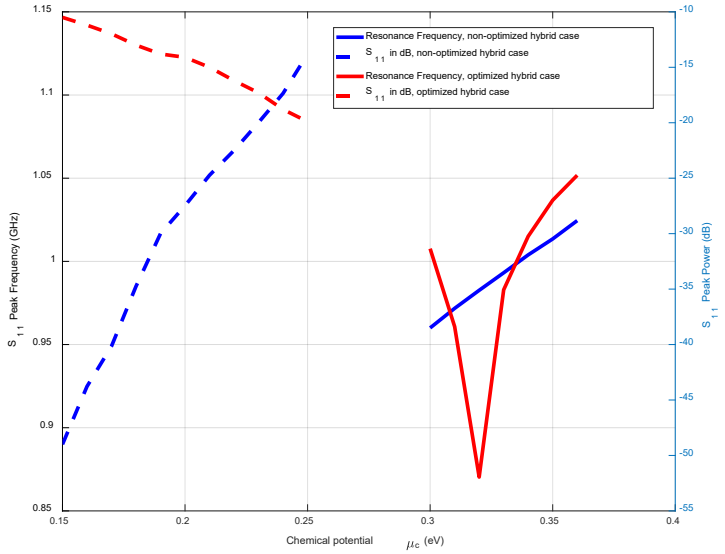

Figure 4.14. Resonant frequency shift and $s_{11}(f)$ as a function of the chemical potential μ_c for hybrid-gold antenna.

One of the highlights of the graphene antenna design is that the conductivity of the graphene can be controlled by a bias tension [Yu13]. Voltage biasing is used to provide more or less electron mobility that produces a shifting on the resonance frequency of the antenna. The same effect can be obtained modifying the chemical potential by adding chemical doping, as micro particles of silver.

Therefore, there are some possibilities to affect the dielectric properties of the graphene which becomes a critical variable for design of some devices, very especially for the antenna design. The availability of a graphene dielectric model including reconfiguration via chemical potential is likewise relevant if the use of simulators is required to optimize some antenna performance parameters. These arrangements can be understood as a graphene property that provides us the reconfiguration capability of the resonant frequency by electronic control. This variable also affects the antenna design and performance, and provides a mean for tuning the resonant frequency.

Among other options, the chemical potential μ_c can be modified by a bias tension. However, this DC voltage bias tuning has limitation due to the breakdown voltage of the material.

The maximum chemical potential $\mu_{c,max}$ that can be applied to keep the material in the so-called safe region is related to the breakdown voltage E_n as follows (4.7):

$$E_n = \frac{q}{\epsilon_0 \epsilon_r} n_s = \frac{q}{\epsilon_0 \epsilon_r} * \frac{1}{\pi} \left(\frac{\mu_{c,max}}{\hbar v_F} \right)^2 \tag{4.7}$$

Therefore $\mu_{c,max}$ is given as in (4.8):

$$\mu_{c,max} = \sqrt{\frac{E_n \epsilon_0 \epsilon_r \pi (\hbar v_F)^2}{q}} \tag{4.8.}$$

where E_n is the breakdown voltage in Volts per meter. As an example, the gallium arsenium GaAS has a breakdown voltage of $E_n = 4e7 \frac{V}{m}$ whence $\mu_{c,max} = 0.180\ eV$.

In **Figure 4.13** the resistance and reactance of the graphene surface impedance R_s is obtained for different values of the chemical potential μ_c. The tuning effect produced by varying the chemical potential μ_c is due to the increasing of the surface charge density n_s which results in a variation of the conductivity σ. The surface charge density n_s is given by (4.9) and exhibits exponential behavior with frequency:

$$n_s(\mu_c) = \frac{2K_B^2}{\pi \hbar^2 v_F^2} \int_0^\infty d\epsilon\, \epsilon \left[f_d(\epsilon) - f_d(\epsilon + 2\mu_c) \right] \tag{4.9}$$

Another possibility of reconfiguration consists of modifying the relaxation time τ and equivalently the relaxation constant τ_s. This parameter can be controlled by increasing the quality of the graphene, so that the charged impurity in the substrate is less and the carrier concentration increases as the Fermi energy does [Ada07]. Then when doping of graphene increased, its relaxation constant τ_s decreased. However, the Fermi energy in graphene can also be tuned via a back gate voltage which results in doping of graphene [Car12][Car13].

The relaxation constant τ_s influences, via the scattering rate γ, the value of the surface conductivity σ and the surface impedance R_s which, at the end, yields a resonant frequency shift of the radiating patch.

For quartz the breakdown voltage is $67 \cdot 10^7$ V/m, using the expression in (4.9) the maximum chemical potential is 0.3972 eV that still lays on the safe region. $\mu_c = 0.34\ eV$.

Keeping the same antenna structure dimensions and performing a sweep of the chemical potential μ_c the antenna can be tuned to 1 THz. In **Figure 4.14** the resonant frequency shift and the value of $s_{11}(f)$ are represented as a function of the chemical potential μ_c. It is observed that the resonant frequency shift fits a linear variation with the chemical potential. However, it should be noticed that the tuning range must be reduced to the interval [0.15, 0.3] eV or a rebound effect will occur.

The reconfiguration via the chemical potential μ_c, attainable by a DC tension bias, would avoid re-optimizing the design in order to obtain physical dimensions of the patch that improves the antenna performance in terms of return loss. This is especially important if the antenna size is critical and must be kept below a limit, as in antenna packaging. We observe that the impedance matching on the tuning range stays over -20dB, that can be assumed as reasonable upon the aimed application.

Finally, although graphene has a number of advantages, when working at room temperatures around 25 degrees and being a monatomic layer, it presents large losses. This means that the radiation pattern has an efficiency of -3dB. Currently there are already multilayer graphene or graphene composed of graphene nanotubes that could improve efficiency [Car13].

4.3 Off-chip antennas

For the off-chip antennas, microstrip design with coplanar placement of radiation elements and feeding network becomes a choice to achieve a functional element with a proper balance of performance (i.e. high gain), compact size and manufacturing complexity for 6G applications [Alv15]. As an example, the 60GHz band corresponding to the WiGig or IEEE 802.11ad standard for vehicular communications [IEEb], among other applications, has been chosen as operation band of the implemented antenna prototypes.

4.3.1 Microstrip array antenna

The purpose of this design has been to obtain an antenna of reduced dimensions (12.28 x 12.28 mm) and a high gain (16 dB simulation 14.4 dB measured) for use in future 5G applications; in case said application requires higher gain must increase the number of patches in the array, in turn increasing its dimensions. To this aim, an array of 16 elements with low-cost microstrip technology has been implemented. The array was manufactured in Rogers RT duroid 5880 due to its low dielectric constant. The elements of the array are rectangular patches fed by inset feed. Due to the small space between patches, the power network has been constructed using triangular power dividers.

The substrate used was Rogers RT Duroid 5880 with ϵ_r=2.20, tanδ=0.0009 and a thickness of 0.381 mm. This thickness was chosen based on the limitations of the milling machine [Alv15].

The array is made up of 16 rectangular patches and for simplicity it is designed as symmetrically as possible; this implies that all patches and feed lines must be symmetrically equal. Likewise, it was sought to achieve a good ratio of secondary lobes and avoid greating lobes, so the distance between elements of the array was tried to be optimized, being this closest to $(\lambda_0/2)$. This was the reason for the implementation of triangular power dividers, having achieved a distance between radiating elements of $0.7 \cdot \lambda_0$.

Initially the array was fed using the connector model 1892-04A-6 from SouthWest Inc. (**Figure 4.15**), choosing the central point of the array backside as the feeding point. The objective of this location was to avoid the influence of the radiation caused by the feed line between the connector and the feeding network.

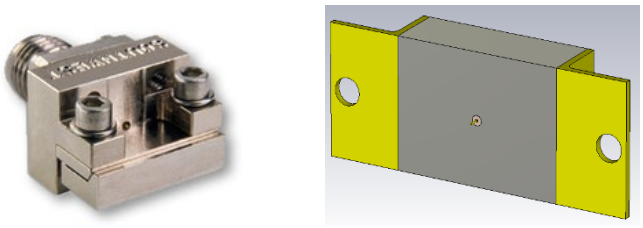

(a) (b)

Figure 4.15. (a) Original connectorl 1892-04A-6, and (b) modified version.

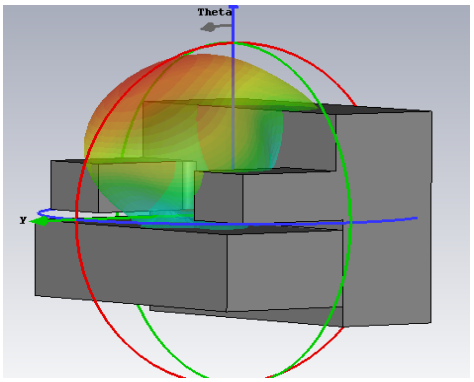

Figure 4.16. Simulation of the radiation due to the feeding connector.

In **Figure 4.16** a simulation demonstrated the radiation due to the connector if a coplanar location was chosen. The connector pin is attached directly to the central feeding line, its impedance being 100Ω, so as the connector sees a 100Ω resistive parallel, a perfect impedance matching is achieved. The subsequent feed lines located below maintain the same impedance value.

All array design parameters were optimized using CST Studio with the goal of achieving the highest possible antenna power gain. Due to the chosen substrate with a value of ϵ_r equal to 2.20 and a thickness of 0.381, the surface currents (**Figure 4.17**) will tend to affect the theoretical values of the dimensions of the elements and therefore a long optimization process was required.

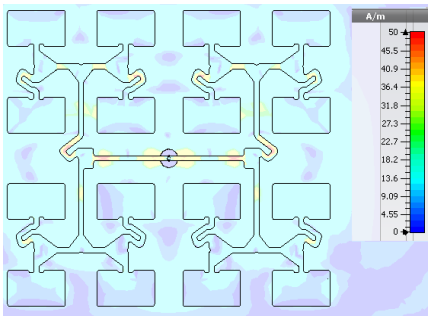

Figure 4.17. Surface currents simulation of the 16-element array antenna.

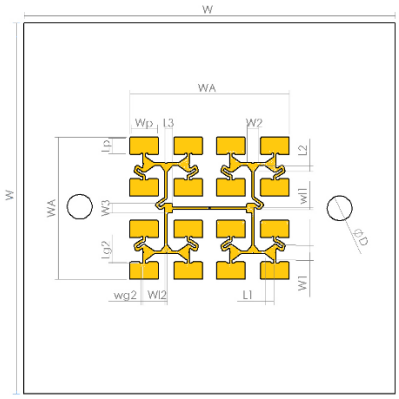

Figure 4.18. Geometry of the 16-element array antenna.

The geometry of the array is shown in **Figure 4.18**. In **Table 4.4** the optimized values of the involved dimensions are summarized.

The antenna was manufactured and assembled with the previously modified connector. The prototype, shown in **Figure 4.19**, was characterized in a compact anechoic chamber especially

designed for small size and high frequency antennas [Exp20] by using a vector network analyzer and a custom developed software at the Antelia Laboratory of the University of Vigo.

Table 4.4. Geometrical parameters of the 16-element array antenna in *mm*.

W	**W_A**	**W_p**	**L_p**	**W_1**	**L_1**	**W_2**	**L_2**	**W_3**	**L_3**
30	12.28	2.15	1.25	1.22	0.72	0.92	0.46	0.78	0.6
W_{l1}	**W_{g2}**	**W_{l2}**	**D**						
0.19	0.2	0.1	2						

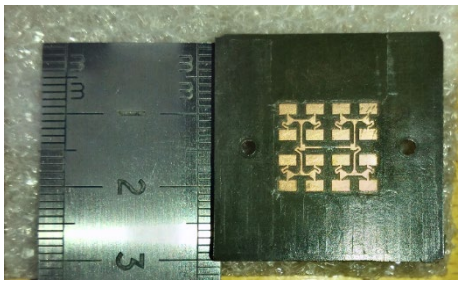

(a)

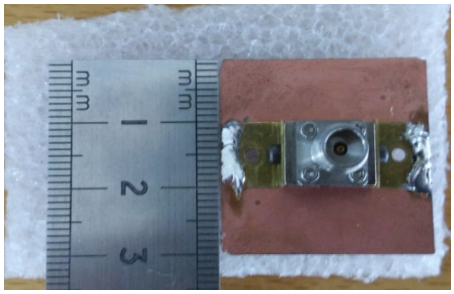

(b)

Figure 4.19. Picture of the fabricated prototype: 8a) frontal and (b) back view.

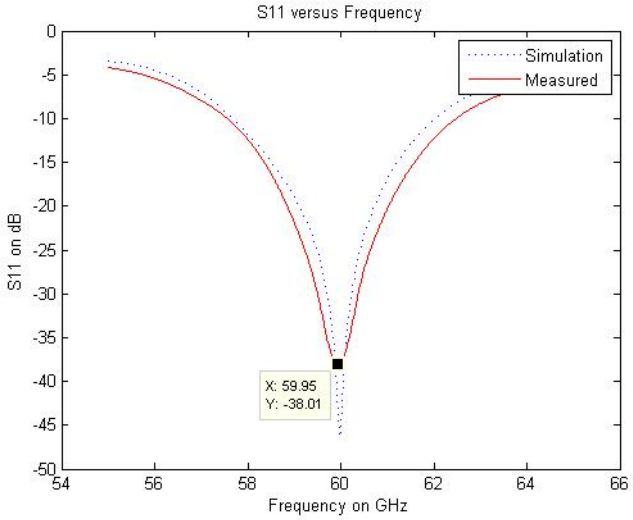

Figure 4.20. s_{11} of the array antenna: simulated (blue) vs measured (red).

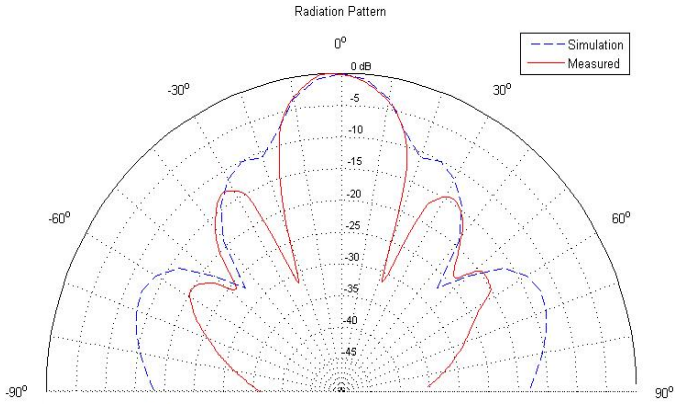

Figure 4.21. Normalized radiation diagram in XZ plane: simulated (blue) vs measured (red).

The main obtained results were:

- a final value of s_{11} of -38 dB at the resonat frequency of almost 60GHz, as shown in **Figure 4.20**;
- a bandwidth of almost 4 GHz, for a criteria of -10dB;
- a radiation pattern (**Figure 4.21**), for $\varphi = 0°$ cut plane, with a main lobe of beamwidth of 100° in simulation and 100° once measured;

almost 15 dB of power gain, as observed in **Figure 4.22**.

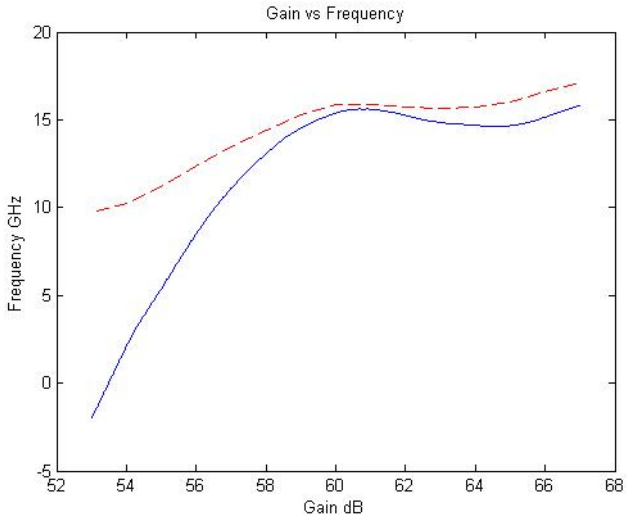

Figure 4.22. Array antenna power gain versus frequency: simulated (blue) vs measured (red)

Based on the measured results, it is concluded that the objective of designing and manufacturing a 60 GHz array with a minimum deviation from the simulation results has been achieved.

The microstrip antennas with coplanar radiation elements and feeding network achieve an enough proper trade-off between performance and manufacturing complexity. Moreover, the choice of Duroid substrate for implementing these microstrip antennas have demonstrated performance results as good as those of LTCC [Che10] [Big11] [Wan13] [Li14] [Alv15].

Through a mechanical manufacturing process we have managed to develop a low cost array. The measurements carried out show a series of differences with respect to the simulation; these differences are due to errors in the manufacturing process, in addition to small variations in the dielectric constant along the substrate. Generally, a number of problems related to the design of a basic microstrip structure have been observed.

A simmetrical array antenna geometry shows less restrictive fabrication needs of resolution and accuracy with respect to other microstrip structures, fabrication restrictions can significantly influence this antenna features, such as resonant frequency and radiation efficiency. However, because the manufacturing process is a mechanical process, it has a series of limitations. The main limitation is the narrowest milling cutter that can be used, in our case and for this milling machine model, it is the Endmill RF 0.15 mm. Therefore the minimum gap distance between array elements (lines or patches) cannot be less than 0.15mm. In addition, the milling cutter not only removes the copper but also mills part of the substrate material and must be taken into account in the simulations, in our case 0.080 mm in thickness height. If this is not entered in the simulation, a deviation of 300 MHz occurs in the center or resonant frequency.

Once the work of designing and manufacturing the array has been completed, the several observed issues can be categorized in three main groups [Alv15]:

i. *Innacurate value of relative dielectric permittivity ε_r:* even commercial substrates used for antenna fabrication do not indicate values of the ε_r beyond 10GHz. This issue becomes a critical question when designing at millimeter wave frequencies, given that the value of ε_r partly determines the geometrical dimensions of the basic patch.

ii. *Connector - feed line soldering:* it is commonly accepted that a soldering introduces noise. Even when not fully analytically modeled, the use of transition stages – soldering points and vias – made of a different metal, represents a not negligeable design issue to be included in the theoretical design.The connector itself becomes a radiating element that can shadow the radiation pattern provided by the patches.

iii. *Fabrication mechanical innacuracies and errors*: in a design it should be considered the minimal dimensions that the fabrication process can achieve as well as the effect on the final result due to the innacuracies and errors shown up in the aimed dimensions.

4.3.2 Bull's eye antenna

This section describes a low-cost leaky-wave millimeter antenna using surface waves propagating on a grounded dielectric. This design is based on previously existing prototypes of antennas implemented entirely in aluminum [Bea15]. However, the design presented here collects the fundamental principles of operation and transfers them to a prototype in microstrip technology at 60 GHz using the Rogers RT Duroid 5880 substrate.

The geometry of the antenna is shown in **Figure 4.23**. As observed, this structure is composed by eight concentric rings with circular microstrip patch that works as a point source of cylindrical surface waves.

The surface wave is generated by the circular microstrip patch, which also provides the circular polarization, and then perturbed into a leaky-wave regime by the gratings structure composed by the microstrip rings.

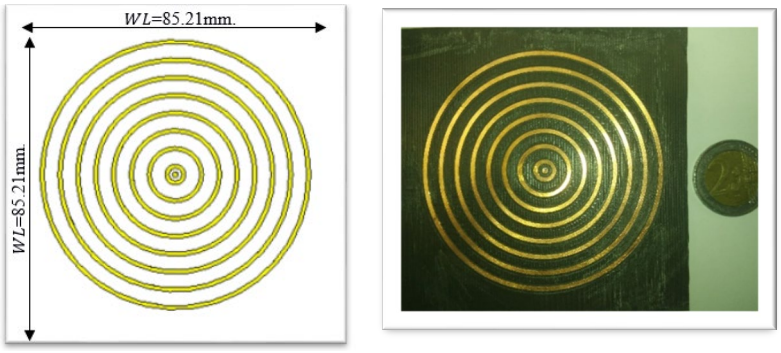

(a) (b)

Figure 4.23. (a) Geometry of the Bull' s eye antenna. (b) Front view of the fabricated prototype.

In first instance, the circular patch is simulated and optimized without the bull's eye rings using CST Microwave Studio as FDTD solver. Next an overall optimization was made both of the rings and of the circular patch, searching the best goal on gain and s_{11}.

A coaxial feeding structure was designed and simulated in order to easy feed the antenna and facilitate its integration and miniaturization in existing devices.

With the aim of achieving a prototype that can be fabricated by mechanical process (LPKF H100 Protomat numerical milling) a substrate with low dielectric constant is chosen, specifically Rogers RT Duroid 5880 with ε_r =2.22 of and $h = 0.381\ \mu m$ of thickness. This low dielectric constant allows to have a feasible dimension on the fabrication process. With this ϵ_r of 2.22 the λ_{eff} is 3.35.

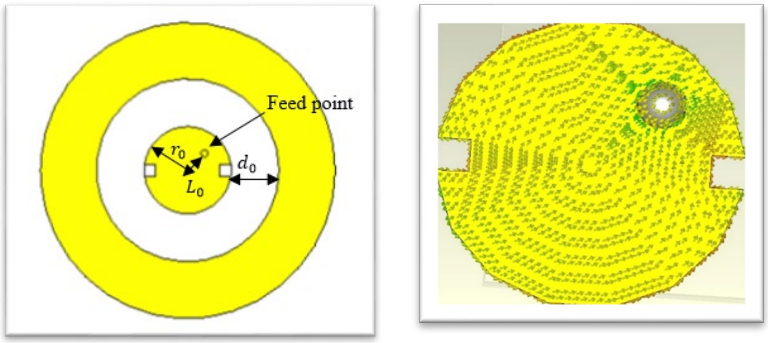

(a) (b)

Figure 4.24. (a) Detail of the radiating central patch.(b) Surface current distribution in the central patch..

As illustrated in **Figure 4.24**, the distance between rings was chosen to satisfy the expression in (4.10):

$$\rho/\lambda_0 > \frac{1}{2} \tag{4.10}$$

In this design $\rho = 4.56$ mm and λ_0 at 60 GHz on air is 5 mm. When ρ is sufficiently large, a fast complex (leaky) wave appears, which gives rise to radiation at some angle between backfire and endfire. The mutual interaction of the rings is responsible for mode-coupling resonances, thus affecting the formation of pass and stop bands, the operating bandwidth, as well as the radiation properties and scan angles. In this design all parameters are optimized to reinforce a low s_{11} at 60 GHz and set the scan angle to zero ergo perpendicular to the plane of the antenna.

The **Figure 4.24** shows in detail the center of the bull's eye antenna and the surface current distribution of the central patch, The feed point is located at distance $L_0 = 0.5245\ mm$ from the center of the antenn on an angle of 45°. This angle provides the circular polarization and the

distance L_0 is result of the optimization process procuring a good impedance matching. The square notches on the patch are not needed in first instance but its provides an enhancement of the bandwidth, and the optimization process set the notches length to 0.2 mm.The rings have a constant width of $w = 0.9958\ mm$.

The distance between rings is constant and fixed to ρ, however the distance between the circular patch and the first ring is quite different $d_0 = 0.8508\ mm$. The number of rings is chosen as an agreement between the surface needed of the antenna and the increment of gain per added ring. The optimal value is set to eight rings with a maximum gain of 19.8 dB.

The prototype was fabricated using mechanical process, in this case a LPKF H100 Protomat numerical milling was used. The substrate used Rogers RT Duroid 5880 includes PTE Teflon for obtain an ϵ_r of 2.22, that makes this material to be really too soft for the milling machine. Then the milling will cause imperfections on the surface of the antenna that affect the final performance due to the impact on s_{11}. The mill causes defects in the shape of the rings, depressions in the substrate, deformations in the circular patch, deformed notches, and an excess of tin. Some of these imperfections can be observed in the **Figure 4.25**.

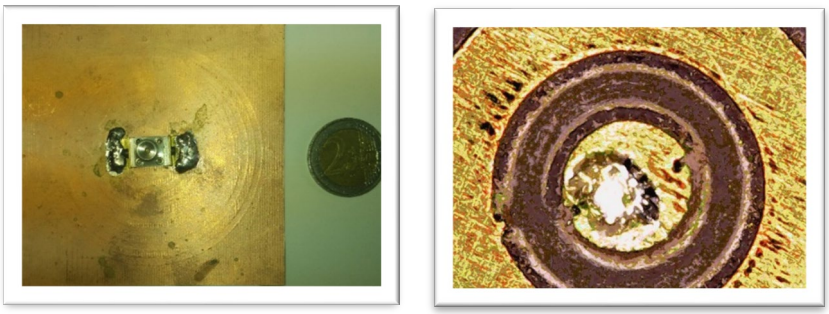

(a) (b)

Figure 4.25. (a) Rear and (b) inspection microscope view of the circular patch.

For the electrical connection at the antenna feeding point, a connector model 1892-04A-6 from Southwest was modified in order to facilitate a rear connection through the ground plane, similarly to the array case described in **Section 4.3.1**. This connector was also introduced in the simulation to reduce possible deviations on the s_{11}.

The final prototype was measured in the same compact anechoic chamber described in Section 4.3.1 for the 16-element array, using a vector network analyzer and a custom developed software at the Antelia Laboratory of the University of Vigo. Even when the measurements were made in the same anechoic chamber and using the same equipment, the s_{11} obtained shows a frequency shift of 3.6 GHz, as shown in the **Figure 4.26**. These deviations are due to poor impedance matching. Zooming in on the radiant element (**Figure 4.25b**) it can be appreciated the level of imperfection of the circular patch in addition to the excess of applied tin.

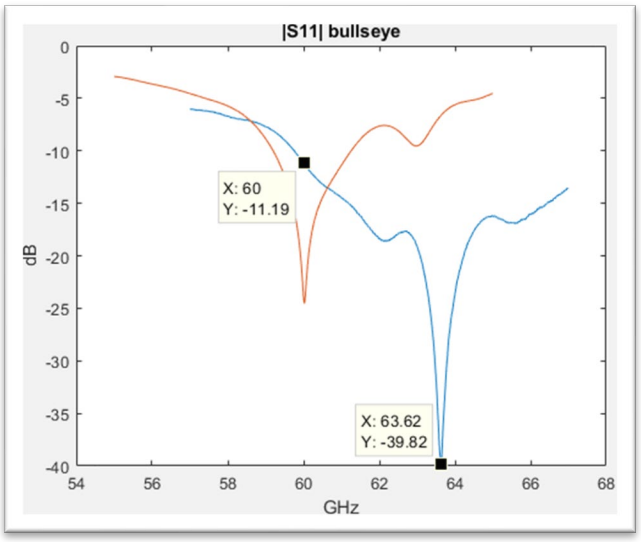

Figure 4.26. s_{11} of the Bull'seye antenna: simulated (red) vs measured (blue).

The imperfections of the fabrication process caused an impedance mismatching favoring the impedance matching of the second resonance that the measured s_{11} only reached a value of -10 dB at the frequency of interest whilst it was of around -25 dB in the simulation.

The measured radiation pattern shown in **Figure 4.27** indicates a main lobe wider (10° of beam width) than the one simulated (6° of beamwidth) but with the same side lobe level (SLL) of -12 dB. As observed in **Figure 4.28**, the vaximum value of the simulated gain was 19.8 dB and the measured one was of 15.6 dB. The antenna resonates at 60 GHz, and that is why it reaches a good level of gain, but due to manufacturing errors or imperfections, a poor adaptation of impedances occurs at the frequency of interest.

Even when this antenna geometry shows less restrictive fabrication needs of resolution and accuracy with respect to other microstrip structures (antenna arrays), fabrication restrictions can significantly influence this antenna, such as resonant frequency and radiation efficiency. For this reason, to obtain better results, some type of laser manufacturing and oven welding or other alternatives should be used.

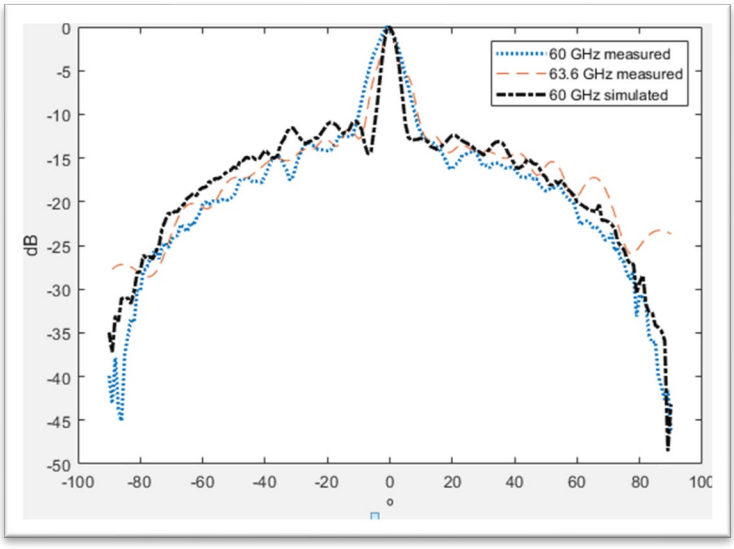

Figure 4.27. Normalized radiation diagrams simulation and measurement.

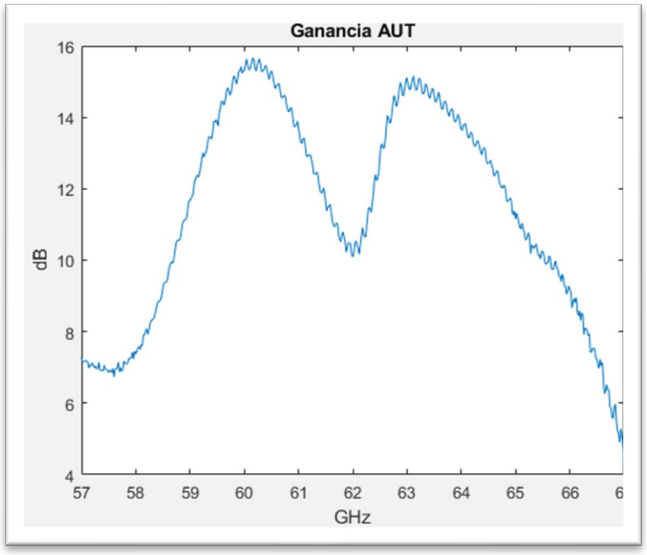

Figure 4.28. Measured gain versus frequency for the Bull'seye antenna.

4.4 Conclusions and Related Publications

The CV-QKD transmitter was provided with a radiofrequency transmission channel in addition to the optical output channel by using photodiodes on the device outputs. To allow radio transmission, the design of two types of antenna solutions has been undertaken: on-chip and off-chip antennas.

The on-chip antennas have been conceptualized to be integrated into the transmitter PIC itself or into an individual chip, on an InP or Si platform. Millimeter bands of 26GHz and 1THz allocated for future 6G systems have been chosen as working frequencies to have effective wavelengths in the substrate small enough to be able to integrate the antenna design in an individual chip and even in the PIC of the transmitter. The achieved designs show a limited but sufficient power gain to allow their use in short-range applications.

The off-chip antennas are proposed for applications requiring longer ranges and higher power gains. Therefore, larger antennas will be achieved that must be located externally to the PIC. Microstrip technology was chosen as the most suitable technology to achieve a compact size, especially for use in millimeter bands applications. The operating frequency proposed of the WiGig or IEEE 802.11ad standard at 60GHz band was selected as resonant frequency.

The innacuraccies observed due to different factors during the design process (connectors, dielectric substrate, milling machine errors,…) have been analyzed, and published an a international conference paper that has received 84 citations so far.

A packaging PCB has been designed provided of coplanar microstrip lines matched in impedance to 50 Ohms for the PIC outputs and inputs, which will be connected to the chip using wire bonding both for a future complete characterization of the transmitter PIC and for testing antennas whose frequency is higher than the modulation baseband and will not be integrated within the PIC.

The main parameters of the designed antennas are summarized in **Table 4.5**.

Table 4.5. Summary of the main antenna parameters.

Substrate / patch	Directivity / Gain (dB)	S_{11} (dB)	ø=0°/90° (°)	SLL (dB)	Dimensions (mm x mm)
InP / Gold	5	-32			
Quartz / Graphene	2				
RT5880 / Cu					
RT5880 / Cu	19.35	-17.37	12	16	12.48